

Optical PAM-4/PAM-8 generation via dual-Raman process in Rydberg atoms

Xiao-Yun Song(宋晓云), Zheng Yin(尹政), Guan-Yu Ren(任冠宇), Ming-Zhi Han(韩明志), Ai-Hong Yang(杨艾红), Yi-Hong Qi(祁义红), and Yan-Dong Peng(彭延东)

Citation: Chin. Phys. B, 2024, 33 (**6**): 064203. DOI: 10.1088/1674-1056/ad3344
Journal homepage: http://cpb.iphy.ac.cn; http://iopscience.iop.org/cpb

What follows is a list of articles you may be interested in

Superradiance of ultracold cesium Rydberg $|65D_{5/2}> \rightarrow |66P_{3/2}>$

Liping Hao(郝丽萍), Xiaoxuan Han(韩小萱), Suying Bai(白素英), Xiufen You(游秀芬), Yuechun Jiao(焦月春), and Jianming Zhao(赵建明)
Chin. Phys. B, 2024, 33 (**5**): 054204. DOI: 10.1088/1674-1056/ad20da

Effectively modulating spatial vortex four-wave mixing in a diamond atomic system

Nuo Ba(巴诺), Ming-Qi Jiang(姜明奇), Jin-You Fei(费金友), Dan Wang(王丹), Hai-Lin Jiang(蒋海林), Lei Wang(王磊), and Hai-Hua Wang(王海华)
Chin. Phys. B, 2024, 33 (**4**): 044202. DOI: 10.1088/1674-1056/ad0771

Monte Carlo simulations of electromagnetically induced transparency in a square lattice of Rydberg atoms

Shang-Yu Zhai(翟尚宇) and Jin-Hui Wu(吴金辉)
Chin. Phys. B, 2021, 30 (**7**): 074206. DOI: 10.1088/1674-1056/abd75a

Nonlinear spectroscopy of three-photon excitation of cesium Rydberg atoms in vapor cell

Jiabei Fan(樊佳蓓), Yunhui He(何云辉), Yuechun Jiao(焦月春), Liping Hao(郝丽萍), Jianming Zhao(赵建明), and Suotang Jia(贾锁堂)
Chin. Phys. B, 2021, 30 (**3**): 034207. DOI: 10.1088/1674-1056/abca25

A sensitive detection of high Rydberg atom with large dipole moment

Shan-Shan Zhang(张珊珊), Hong Cheng(成红), Pei-Pei Xin(辛培培), Han-Mu Wang(王汉睦), Zi-Shan Xu(徐子珊), Hong-Ping Liu(刘红平)
Chin. Phys. B, 2018, 27 (**7**): 074207. DOI: 10.1088/1674-1056/27/7/074207

Optical PAM-4/PAM-8 generation via dual-Raman process in Rydberg atoms

Xiao-Yun Song(宋晓云)[1], Zheng Yin(尹政)[1], Guan-Yu Ren(任冠宇)[1], Ming-Zhi Han(韩明志)[3], Ai-Hong Yang(杨艾红)[1,‡], Yi-Hong Qi(祁义红)[2,§], and Yan-Dong Peng(彭延东)[1,†]

[1] *Qingdao Key Laboratory of Terahertz Technology, College of Electronic and Information Engineering, Shandong University of Science and Technology, Qingdao* 266590, *China*

[2] *School of Physics, East China University of Science and Technology, Shanghai* 200237, *China*

[3] *MIIT Key Laboratory of Complex-field Intelligent Exploration, Beijing Institute of Technology, Beijing* 100081, *China*

(Received 21 December 2023; revised manuscript received 3 March 2024; accepted manuscript online 13 March 2024)

A scheme of optical four-level pulse amplitude modulation (PAM-4) is proposed based on dual-Raman process in Rydberg atoms. A probe field counter-propagates with a dual-Raman field which drives the ground and the excited states transition, respectively, and the Rydberg transition is driven by a microwave (MW) field. A gain peak appears in the probe transmission and is sensitive to the MW field strength. Optical PAM-4 can be achieved by encoding an MW signal and decoding the magnitude of a probe signal. Simulation results show that the differential nonlinearity and the integral nonlinearity of the proposed scheme can be reduced by 5 times and 6 times, respectively, compared with the counterparts of previous scheme, and the ratio of level separation mismatch is close to the ideal value 1. Moreover, the scheme is extended to optical PAM-8 signal, which may further improve the spectral efficiency.

Keywords: Rydberg atoms, PAM-4/PAM-8, dual-Raman process

PACS: 42.50.Gy, 32.80.Qk, 32.80.Ee, 42.50.Ex **DOI:** 10.1088/1674-1056/ad3344

1. Introduction

Advanced modulation formats have attracted great attention for their ability to enhance the data transmission rate.[1–5] For example, four-level pulse amplitude modulation (PAM-4) is the preferred modulation format in the 400-Gb/s short-reach optical communication systems due to its higher spectral efficiency.[6,7] Rydberg atoms offer the possibility of superiority over the traditional dipole antennas for classical digital communication because they may lead to parallel and fast communication avoiding internal thermal noise. For example, microwave (MW) communication based on Rydberg atoms has the advantages of long transfer distance, large data transfer capacity, and high transfer quality. Therefore, electromagnetic-induced transparency (EIT) scheme based on Rydberg atoms arouses great interest in amplitude modulation,[8,9] phase shift key,[10,11] frequency modulation,[12,13] phase modulation,[14,15] MW electric-field measurement,[16–22] etc. Also, we notice that some other researches of Rydberg atoms, such as Rydberg blockade effect,[23,24] Rydberg-atom array,[25,26] and Rydberg spectroscopy.[27,28]

Optical PAM-4 signal is often obtained by electrical modulation, such as Mach–Zehnder modulator and graphene-based adaptive modulator. Samani *et al*. designed an O-band modulator based on Mach–Zehnder interferometer and studied a 400-Gb/s short-reach transmission system modulated by PAM-4.[29] Camacho *et al*. presented a new concept of a graphene-based adaptive modulator for multilevel amplitude modulation on polymer technology platform, combined electro-optical characteristics.[30] Coherent control optical modulation provides a new way for PAM-4. The Rydberg-atom-based microwave receiver combined with the classical modulation and demodulation technology also has been used in the receiving antenna of wireless signals. In analogue to classical communication, Deb *et al*. demonstrated the radio over fiber (RoF) of radio frequency signals based on EIT in Rydberg atoms.[31] Anderson *et al*. used atomic antennas to receive and restore the audio signals loaded by amplitude modulation or frequency modulation.[32] In terms of digital communication, Meyer *et al*. demonstrated phase-sensitive conversion of amplitude-modulated MW signal into optical signal and implemented an 8-state phase-shift-keying digital communication protocol.[8] Wang *et al*. theoretically analyzed the PAM-4 scheme by using phase-dependent EIT in a closed system, exhibiting robustness of the nitrogen-vacancy (NV) system.[14] While, few researches involve MW signal modulation in Rydberg atoms drived by a dual-Raman field.

In this paper, we propose a scheme of optical PAM-4 by using dual-Raman process to modulate the amplitude of MW field in Rydberg atoms. The probe field counter-propagates with respect to the dual-Raman field, and they drive the ground and the excited states transition, respectively. An absorption

†Corresponding author. E-mail: pengyd@sdust.edu.cn
‡Corresponding author. E-mail: yangah_phys@163.com
§Corresponding author. E-mail: qiyihong@ecust.edu.cn

© 2024 Chinese Physical Society and IOP Publishing Ltd

peak appears in the probe transmission in the presence of an MW field. The absorption peak is sensitive to the MW field strength, and the gain of probe field is obtained by modulating the strength of the MW field. The PAM-4 signal appears in the probe transmission. The numerical results show that the differential nonlinearity (DNL) and the integral nonlinearity (INL) can be reduced by about 5 times and 6 times, respectively, compared with those of the NV centers, and the ratio of level separation mismatch (RLM) is closer to the ideal value of 1. Furthermore, we investigate the generation of the optical PAM-8 signal in Rydberg atoms. The proposed scheme is based on the constructive interference between two Raman transitions, which could suppress the absorption of the weak probe field, leading to the increase of transmission and then causing the gain to increase. This is different from the single Raman scheme.[14,19] The scheme may be useful for MW optical communication.

2. Model and basic equations

The Rydberg atomic system we considered is shown in Fig. 1(a). The states $|1\rangle$, $|2\rangle$, $|3\rangle$, and $|4\rangle$ correspond to the rubidium-87 atomic levels $5S_{1/2}$ ($F=2$), $5P_{3/2}$ ($F=3$), $53D_{5/2}$, and $54P_{5/2}$, respectively. The dual-Raman fields Ω_{R1} and Ω_{R2} drive the transition $|2\rangle \to |3\rangle$ with frequency difference $\omega_{R1}-\omega_{R2}=\delta$. A weak probe field Ω_P drives the transition $|1\rangle \to |2\rangle$, and an MW field Ω_M drives the Rydberg transition $|3\rangle \to |4\rangle$. Here, the Rabi frequencies of the corresponding fields are defined as $\Omega_P = E_P\mu_{12}/\hbar$, $\Omega_{R1(R2)} = E_{R1(R2)}\mu_{23}/\hbar$, and $\Omega_M = E_M\mu_{34}/\hbar$ with their electrical magnitudes E_P, $E_{R1(R2)}$, and E_M, with μ_{ij} being the transition dipole moment from state $|i\rangle$ to state $|j\rangle$ ($i,j\in\{1,2,3,4\}$).

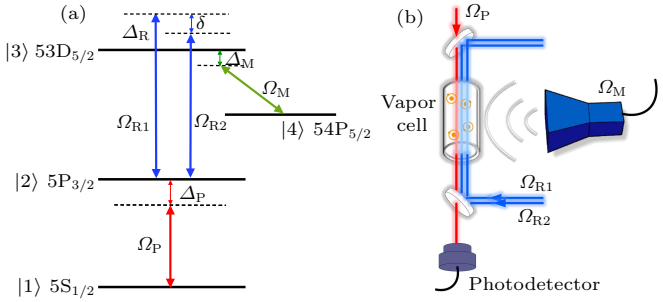


Fig. 1. (a) Four-level Rydberg atom and (b) its coupling scheme.

In the electric dipole approximation, the Hamiltonian of system in the interaction picture is given by[33]

$$H=\hbar\begin{pmatrix} 0 & -\Omega_P & 0 & 0 \\ -\Omega_P & -\Delta_P & -\Omega_{R1}-\Omega_{R2}\,e^{i\delta t} & 0 \\ 0 & -\Omega_{R1}-\Omega_{R2}\,e^{-i\delta t} & -\Delta_P-\Delta_R & -\Omega_M \\ 0 & 0 & -\Omega_M & -\Delta_P-\Delta_R+\Delta_M \end{pmatrix}, \tag{1}$$

where $\Delta_P=\omega_P-\omega_{21}$, $\Delta_R=\omega_{R1}-\omega_{32}$, and $\Delta_M=\omega_M-\omega_{43}$ are the detuning of the probe, Raman, and MW fields, respectively, with ω_{ij} being the transition frequency from $|i\rangle$ to $|j\rangle$ ($i,j\in\{1,2,3,4\}$). The dynamic evolution of the system can be described by solving the density master equation[34]

$$\frac{\partial\rho}{\partial t}=-\frac{i}{\hbar}[H,\rho]+L(\rho), \tag{2}$$

where $L(\rho)$ denotes the decoherence processes. And then the time evolutions of density matrix elements are given as follows:

$$\begin{aligned}
\dot\rho_{21} &= -\gamma_{21}\rho_{21}-i\big[-\Delta_P\rho_{21}+\Omega_P(\rho_{22}-\rho_{11}) \\
&\quad +(-\Omega_{R1}-\Omega_{R2}\,e^{i\delta t})\rho_{31}\big], \\
\dot\rho_{31} &= -\gamma_{31}\rho_{31}-i\big[(-\Delta_P-\Delta_R)\rho_{31}+\Omega_P\rho_{32}-\Omega_M\rho_{41} \\
&\quad +(-\Omega_{R1}-\Omega_{R2}\,e^{-i\delta t})\rho_{21}\big], \\
\dot\rho_{41} &= -\gamma_{41}\rho_{41}-i\big[(-\Delta_P-\Delta_R+\Delta_M)\rho_{41} \\
&\quad +\Omega_P\rho_{42}-\Omega_M\rho_{31}\big],
\end{aligned} \tag{3}$$

with the closure relationship $\rho_{11}+\rho_{22}+\rho_{33}+\rho_{44}=1$, $\gamma_{jk}=(\Gamma_j+\Gamma_k)/2$, and $\Gamma_j=\sum_k\Gamma_{jk}$ $(j,k=1,2,3,4)$, where Γ_{jk} is the spontaneous decay rate from state $|j\rangle$ to state $|k\rangle$. We perform a rotating-frame transformation by using $\rho_{21}=\tilde\rho_{21}\,e^{-i\omega_P t}$, $\rho_{31}=\tilde\rho_{31}\,e^{-i(\omega_P+\omega_{R1})t}$, and $\rho_{41}=\tilde\rho_{41}\,e^{-i(\omega_P+\omega_{R1}-\omega_M)t}$. The density-matrix element $\tilde\rho_{ij}$ can be expanded in terms of Fourier components as

$$\tilde\rho_{ij}=\sum_n\tilde\rho_{ij}^{(n)}\,e^{-in\delta t}\quad(i,j\in\{1,2,3,4\},n=0,\pm1,\ldots). \tag{4}$$

We keep the first order of the probe and all orders of the dual-Raman and MW fields, and then we obtain

$$\begin{aligned}
\tilde\rho_{21}^{(n)} &= \frac{i(\Omega_P+\Omega_{R1}\tilde\rho_{31}^{(n)}+\Omega_{R2}\tilde\rho_{31}^{(n+1)})}{\gamma_{21}-i\Delta_P-in\delta}, \\
\tilde\rho_{31}^{(n)} &= \frac{i(\Omega_M\tilde\rho_{41}^{(n)}+\Omega_{R1}\tilde\rho_{21}^{(n)}+\Omega_{R2}\tilde\rho_{21}^{(n-1)})}{\gamma_{31}-i(\Delta_P+\Delta_R)-in\delta}, \\
\tilde\rho_{41}^{(n)} &= \frac{i\Omega_M\tilde\rho_{31}^{(n)}}{\gamma_{41}-i(\Delta_P+\Delta_R-\Delta_M)-in\delta}.
\end{aligned} \tag{5}$$

The solution of $\tilde\rho_{21}^{(n)}$ is obtained from the recursion relation

$$\tilde\rho_{21}^{(n)}=P_n^{-1}\left(-i\Omega_P+\frac{\Omega_{R1}^*\Omega_{R2}\tilde\rho_{21}^{(n-1)}}{X_n}+\frac{\Omega_{R1}\Omega_{R2}^*\tilde\rho_{21}^{(n+1)}}{X_{n+1}}\right), \tag{6}$$

where

$$\begin{aligned}
P_n &= i(\Delta_P+n\delta)-\gamma_{21}-\frac{\Omega_{R1}^2}{X_n}-\frac{\Omega_{R2}^2}{X_{n+1}}, \\
X_n &= \gamma_{31}-i(\Delta_P+\Delta_R+n\delta) \\
&\quad +\frac{\Omega_M^2}{\gamma_{41}-in\delta+i(\Delta_M-\Delta_P-\Delta_R)}.
\end{aligned} \tag{7}$$

The coherent term $\tilde{\rho}_{21}^{(0)}$ indicates the linear absorption and dispersion properties of the system and can be obtained by using a continued fraction method[35]

$$\tilde{\rho}_{21}^{(0)} = \frac{-\mathrm{i}\Omega_{\mathrm{P}}}{P_0 - \dfrac{\Omega_{\mathrm{R1}}^{*}\Omega_{\mathrm{R2}}W_1}{\gamma_{31} - \mathrm{i}\left(\Delta_{\mathrm{P}} + \Delta_{\mathrm{R}}\right) + \dfrac{\Omega_{\mathrm{M}}^2}{\gamma_{41} - \mathrm{i}\left(\Delta_{\mathrm{P}} + \Delta_{\mathrm{R}} - \Delta_{\mathrm{M}}\right)}} - \dfrac{\Omega_{\mathrm{R1}}\Omega_{\mathrm{R2}}^{*}V_1}{\gamma_{31} - \mathrm{i}\left(\Delta_{\mathrm{P}} + \Delta_{\mathrm{R}} + \delta\right) + \dfrac{\Omega_{\mathrm{M}}^2}{\gamma_{41} - \mathrm{i}\left(\Delta_{\mathrm{P}} + \Delta_{\mathrm{R}} - \Delta_{\mathrm{M}} + \delta\right)}}}, \tag{8}$$

where $W_1 = \tilde{\rho}_{21}^{(1)}/\tilde{\rho}_{21}^{(0)}$ and $V_1 = \tilde{\rho}_{21}^{(1)}/\tilde{\rho}_{21}^{(2)}$. The real part and imaginary part of χ correspond to the dispersion and the absorption, respectively, and are related to $\tilde{\rho}_{21}^{(0)}$ by the polarization relation $P = \varepsilon_0\chi E_{\mathrm{P}}\,\mathrm{e}^{-\mathrm{i}\omega_{\mathrm{P}}t} + \mathrm{c.c.} = \mu_{21}N\tilde{\rho}_{21}^{(0)}\,\mathrm{e}^{-\mathrm{i}\omega_{\mathrm{P}}t} + \mathrm{c.c.}$ The susceptibility χ is found to be $\chi = N\mu_{21}^2\tilde{\rho}_{21}^{(0)}/(\hbar\varepsilon_0\Omega_{\mathrm{P}})$, where ε_0 is the permittivity of vacuum, N is the atomic density, and $\hbar$ is the reduced Planck's constant. The transmission coefficient of the probe field propagating through the atomic vapor cell can be expressed as[36]

$$\left|T'\right| = \exp\left(-\frac{2\pi l\,\mathrm{Im}\left[\chi\right]}{2\lambda_{\mathrm{P}}}\right), \tag{9}$$

where l is the length of the cell and λ_{P} is the wavelength of the probe laser. The probe transmission is given by

$$I_{\mathrm{out}} = I_{\mathrm{P}}T = I_{\mathrm{P}}\left|T'\right|^2 = I_{\mathrm{P}}\exp\left(-\frac{2\pi l\,\mathrm{Im}\left[\chi\right]}{\lambda_{\mathrm{P}}}\right), \tag{10}$$

where I_{P} is the intensity of the incident probe field.

The output field I_{out} and incident field I_{P} can be expressed as

$$I_{\mathrm{out}} = E_{\mathrm{out}}^2, \quad I_{\mathrm{P}} = E_{\mathrm{P}}^2, \tag{11}$$

where E_{P} and E_{out} are the magnitudes of incident field and output field, respectively. The gain of the transmission field is given by $G = \sqrt{\Omega_{\mathrm{P}}^2\left|T'\right|^2}$.

3. Results and discussion

We consider the ^{87}Rb atoms within a 5.0-cm-long vapor cell. In the following discussion, the parameters are scaled by the decay rate $\Gamma = \gamma_{21} = 2\pi \times 6$ MHz for simplicity. We first investigate the variations of the absorption peak and the gain spectra with the MW field Ω_{M}, respectively. Figure 2(a) shows that the absorption peak of the medium changes with MW field in the far-detuned dual-Raman process, i.e., $\Delta_{\mathrm{R}} = -50\Gamma$. The absorption peak decreases with MW field, and reaches a minimum value in a range of 0–20Γ when $\Omega_{\mathrm{M}} \approx 20\Gamma$. Figure 2(b) shows the absorption peaks with different values of MW field Ω_{M}. It is easy to see that the absorption peak at resonant frequency gradually decreases with the increase of Ω_{M}. This indicates that the probe absorption can be modulated by the MW field.

In order to encode the digital information, figure 2(b) shows the absorption spectrum obtained by different MW fields. The probe field will experience different gains through the vapor cell, and the output signal has different power levels which correspond to the encoding information of 00, 01, 10, 11. In other words, the amplitude-controlled gain maps the output signal, which could be used to analyze the spectrum PAM-4 signal.

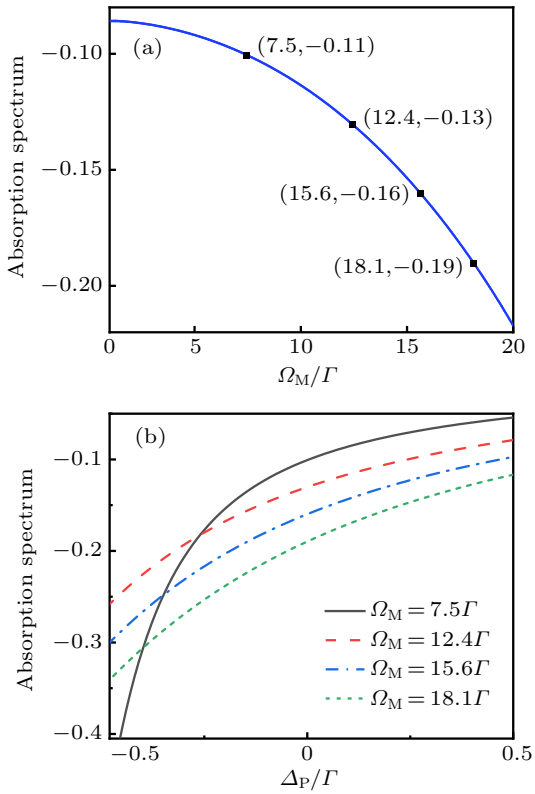


Fig. 2. (a) Absorption spectrum as a function of MW field and (b) with different MW fields. $\Omega_{\mathrm{R1(R2)}} = 10\Gamma$, $\Delta_{\mathrm{M}} = -50\Gamma$, $\Delta_{\mathrm{R}} = -50\Gamma$, $\delta = 20\Gamma$, $\Gamma = \gamma_{21} = 2\pi \times 6$ MHz, $\gamma_{31} = 2\pi \times 1$ kHz, and $\gamma_{41} = 2\pi \times 0.5$ kHz.

The gain effect for probe field can be understood by using the population dynamics. In the scheme, the probe field and dual-Raman field counter-propagate through the atomic vapor, driving atoms from the ground state $|1\rangle$ to the Rydberg state $|3\rangle$. With the coupling of the microwave field Ω_{M}, some atoms are transferred to the Rydberg state $|4\rangle$ through the two-photon Raman resonance, and then they relax to the ground state $|1\rangle$. Since the Raman field has a large frequency detuning, the pump effect from the state $|2\rangle$ to the Rydberg state $|3\rangle$ is limited, and some atoms accumulate at the state $|2\rangle$. So there is some population inversion between the ground state $|1\rangle$ and the excited state $|2\rangle$. When the probe field propagates through the atomic system, coupling the transition $|1\rangle \leftrightarrow |2\rangle$,

the output field is amplified and modulated, i.e., there appears a gained optical PAM-4 signal, so there is a gain effect for the probe field as shown in Fig. 2.

Based on the sensitivity of gain spectrum to the MW field above, the gain spectrum may be used to encode digital signals. Figure 3(a) shows the effect of the MW field on the gain property of the medium in the far-detuned dual-Raman process. The gain peak increases with MW field increasing. For example, when $\Omega_{\rm M} \approx 20\Gamma$, the gain is close to 1.2. So, the magnitude of gain spectrum can be well modulated by tuning the MW field. Figure 3(b) shows that the gain is encoded into 4 states and encoded 2 bits per state from 00 to 11. Signal contrast is defined as the difference between the maximum magnitude and minimum magnitude of the PAM-4 signal. For example, the digital information 00, 01, 10, and 11 are encoded into the transmission signal when the MW field takes 8.2Γ, 16.2Γ, 18.2Γ, and 19.3Γ, respectively.

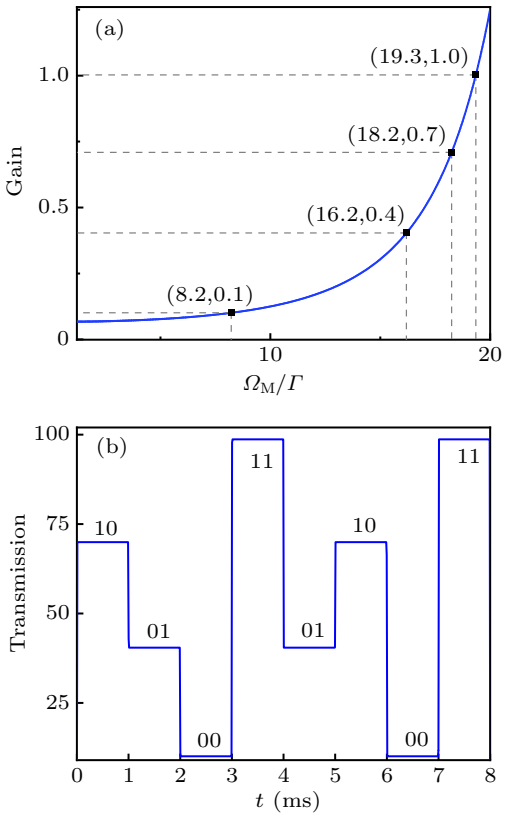


Fig. 3. (a) Gain spectrum changing with MW field and (b) optical PAM-4 signal, with the other parameters being the same as those in Fig. 2.

It is known that the linearity is an important index to evaluate the performance of a PAM-4 transmitter. Here, we calculate DNL and INL of the dual-Raman scheme with Rydberg atoms.[37] The DNL is defined as the difference between the actual analog step and ideal value of the least-significant bit (LSB), which can be expressed as[29]

$$\mathrm{DNL} = \left| \frac{I_n - I_{n-1}}{I_{\rm LSB}} - 1 \right|, \tag{12}$$

where I_n is the amplitude of the level n $(n = 0, 1, 2, 3, \ldots)$, and $I_{\rm LSB}$ denotes the ideal spacing between two adjacent output values.[29,38] We take $I_{\rm LSB} = 30$ and all steps have equal $I_{\rm LSB}$. The DNL $\leq 1_{\rm LSB}$ means that there is no code loss when the Rydberg atom system generates the optical PAM-4 signal. The INL is the difference between the actual transfer function and the ideal case in the longitudinal direction, and can be written as

$$\mathrm{INL} = \left| \frac{I_n - I_0}{I_{\rm LSB}} - n \right|, \tag{13}$$

where the transfer function is defined as the ratio of the output magnitude E to the input $E_{\rm P}$. RLM is a key performance matrix for PAM-4 transmitter, where the minimum value of RLM is required to be at least 95% in many applications. It indicates that the vertical linearity of the signal is a measurement for mismatch between PAM-4 levels. The RLM can be expressed as[39]

$$\mathrm{RLM} = \frac{\min\left(I_n - I_{n-1}, I_{n-1} - I_{n-2}, \ldots, I_1 - I_0\right)}{(I_n - I_0)/n}, \tag{14}$$

where I_i represents an i-th voltage level of a PAM-4 symbol. The numerator is the minimum value among differences between adjacent voltage levels. The denominator is the quotient obtained by dividing the difference between the highest voltage level (I_n) and the lowest (I_0) by n. For an ideal case, RLM = 1, which means that the system is perfectly linear. On the other hand, if the system turns distorted due to non-linearity, the RLM becomes smaller than 1. For example, PAM-4 signal typically requires a minimum RLM to be at least 92% in many applications.[40–42]

For the proposed PAM-4 scheme, the different MW fields are applied here, e.g., $\Omega_{\rm M} = 8.2\Gamma$, 16.2Γ, 18.2Γ, and 19.3Γ, and then the optical PAM-4 signals are obtained with magnitudes of 10, 40, 70, and 100, respectively as shown in Fig. 3(b). The numerical result shows that a most uniform power level of optical PAM-4 signal can be obtained by modulating the MW field. The calculated DNL and INL for the system are 1.9×10^{-4} and 1.3×10^{-4}, respectively. This means that the DNL and INL are about 5 times and 6 times smaller than those of the phase-control scheme,[14] respectively. Moreover, the RLM of the system is about 99.98% obtained from simulation which is closer to the ideal value of 1. Thus, the linearity of the amplitude-dependent dual-Raman scheme is higher than the phase-control scheme. Here, the interference between two Raman channels leads to the gain effect in the probe field, which further amplifies the digital signal and benefits the modulation of PAM-4 signal.

We further investigate the influence of the dual-Raman field on the PAM-4 signal. Figure 4(a) shows that the gain becomes larger as dual-Raman field decreases. For example, the

gain spectrumrises from 0–0.6 to 0–2.7 with $\Omega_{\mathrm{R1(R2)}}$ increasing from 10.5Γ to 9.5Γ. The magnitudes of the digital signals 01, 10, and 11 become larger while the magnitude of the digital signal 00 remains nearly constant. So, the contrast of the PAM-4 signal becomes larger when the dual-Raman field $\Omega_{\mathrm{R1(R2)}}$ becomes weak. For example, the contrast of PAM-4 increases from 30 to 50 when $\Omega_{\mathrm{R1(R2)}}$ decreases from 10Γ to 9.5Γ as shown in Fig. 4(b). This indicates that a relatively weak dual-Raman field may help to improve the signal contrast.

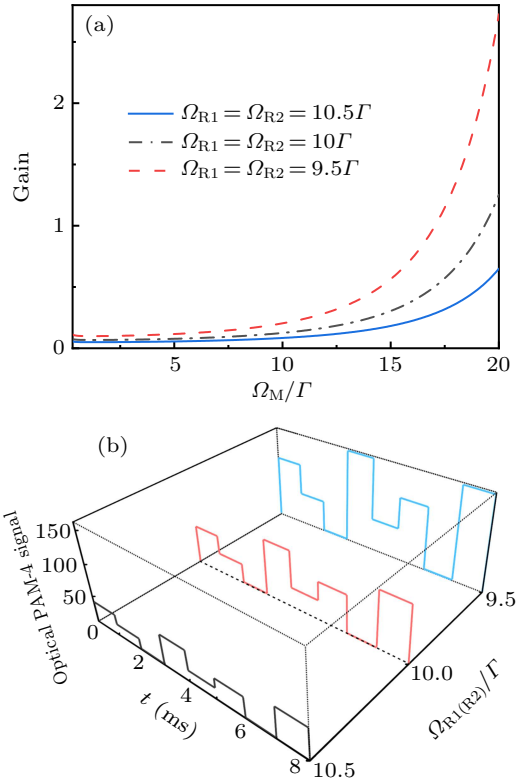


Fig. 4. (a) Gain with different dual-Raman fields and (b) optical PAM-4 signals, with the other parameters being the same as those in Fig. 2.

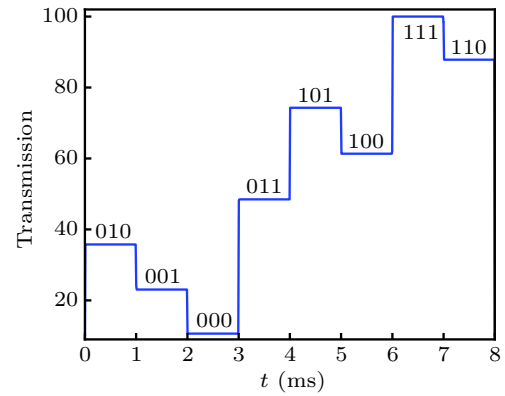


Fig. 5. Optical PAM-8 signal, with the other parameters being the same as those in Fig. 2.

Finally, we investigate the optical PAM-8 signal in the Rydberg atoms as shown in Fig. 5. In order to encode the 8-level digital signal, we choose the MW field $\Omega_{\mathrm{M}} = 8.1\Gamma$, 13.7Γ, 15.7Γ, 16.9Γ, 17.7Γ, 18.4Γ, 18.9Γ, and 19.3Γ to encode the digital signal, respectively. Optical PAM-8 signals of 000–111 are obtained. Of course, the linearity and RLM of the system are sacrificed when realizing multi-level digital communication. The DNL and INL of PAM-8 signal are 2.8×10^{-3} and 1.9×10^{-3}, respectively. The DNL and INL of PAM-8 signal are one order of magnitude lower than those of PAM-4 signal. The RLM of PAM-8 is 99.72%. So, a higher order PAM needs a more linear system, which may benefit for a large RLM of pulse amplitude modulation.

4. Conclusions

In this work, we theoretically analyzed the PAM-4 signal scheme by using the dual-Raman process in Rydberg atoms. Different MW field leads to different absorptions of the Rydberg atoms, which further modilates the gain spectrum. Optical PAM-4 signal can be achieved by encoding the MW signal and decoding the magnitude of the probe signal. The simulation results show that the DNL and INL are about 5 times and 6 times smaller than those of the previous scheme, respectively, and the RLM is closer to the ideal value of 1. Moreover, we investigated the generation of optical PAM-8 signal. This scheme allows us to further improve the signal contrast by tuning the dual-Raman field. The dual-Raman field scheme exhibits high sensitivity, high contrast, and may be useful for MW-optical signal modulation.

Acknowledgements

Project supported by the Shandong Natural Science Foundation, China (Grant No. ZR2021LLZ006), the National Natural Science Foundation of China (Grant Nos. 61675118 and 12274123), the Taishan Scholars Program of Shandong Province, China (Grant No. ts20190936), and the Shandong University of Science and Technology Research Fund, China (Grant No. 2015TDJH102).

References

[1] Li H, Balamurugan G, Sakib M, Sun J, Driscoll J, Kumar R, Jayatilleka H, Rong H, Jaussi J and Casper B 2020 *J. Lightwave Technol.* **38** 131
[2] Feng N and Sun X 2020 *Opt. Commun.* **457** 124609
[3] Mukherjee R, Mallick K, Kuiri B, Santra S, Dutta B, Mandal P and Patra A S 2020 *Opt. Commun.* **476** 126304
[4] Sun L, Du J, Liu J, Chen B, Xu K, Liu B, Lu C and He Z 2019 *J. Lightwave Technol.* **37** 6133
[5] Van Kerrebrouck J, Pang X, Ozolins O, Lin R, Udalcovs A, Zhang L, Li H, Spiga S, Amann M C, Gan L, Tang M, Fu S, Schatz R, Jacobsen G, Popov S, Liu D, Tong W, Torfs G, Bauwelinck J, Chen J and Yin X 2019 *J. Lightwave Technol.* **37** 356
[6] Farzan K and Johns D A 2004 *IEEE J. Solid-State Circuits* **39** 529
[7] Zhong K, Zhou X, Gui T, Tao L, Gao Y, Chen W, Man J, Zeng L, Lau A P T and Lu C 2015 *Opt. Express* **23** 1176
[8] Meyer D H, Cox K C, Fatemi F K and Kunz P D 2018 *Appl. Phys. Lett.* **112** 211108
[9] Yuan J, Jin T, Xiao L, Jia S and Wang L 2023 *IEEE Antennas Wirel. Propag. Lett.* **22** 2580
[10] Pradosh K N, Adwaith K V, Meena M S and Narayanan A 2021 *Appl. Phys. Lett.* **118** 064001
[11] Zhang F, Qi Y and Li W 2019 *Results in Phys.* **13** 102096

[12] Jiao Y, Han X, Fan J, Raithel G, Zhao J and Jia S 2019 *Appl. Phys. Express* **12** 126002
[13] Holloway C L, Gordon J A, Simons M T and Kautz M D 2018 *J. Appl. Phys.* **123** 203105
[14] Wang J, Han M, Zhao S, Cai Y, Jelezko F, Jia Z, Zeng Q and Peng Y 2021 *Results in Phys.* **30** 104802
[15] Liu X B, Jia F D, Zhang H Y, Mei J, Liang W C, Zhou F, Yu Y H, Liu Y, Zhang J, Xie F and Zhong Z P 2022 *Chin. Phys. B* **31** 090703
[16] Xia K, Johnsson M, Knight P L and Twamley J 2016 *Phys. Rev. Lett.* **116** 023601
[17] Zhang S, Hu Y, Lin G, Niu Y, Xia K, Gong J and Gong S 2018 *Nat. Photon.* **12** 744
[18] Simons M T, Gordon J A, Holloway C L, Anderson D A, Miller S A and Raithel G 2016 *Appl. Phys. Lett.* **108** 174101
[19] Peng Y, Wang J, Yang A, Jia Z, Li D and Chen B 2018 *J. Opt. Soc. Am. B* **35** 2272
[20] Fan H, Kumar S, Sedlacek J, Kübler H, Karimkashi S and Shaffer J P 2015 *J. Phys. B: At. Mol. Opt. Phys.* **48** 202001
[21] Gong T, Shi S, Ji Z, Guo G, Sun X, Tian Y, Qiu X, Li C, Zhao Y and Jia S 2023 *Chin. Phys. B* **32** 103202
[22] Zhang L, Liu J, Jia Y, Zhang H, Song Z and Jia S 2018 *Chin. Phys. B* **27** 033201
[23] Cheng Y, Li C and Zhai H 2023 *New J. Phys.* **25** 033010
[24] Guo S, Huang J, Hu J and Li Z X 2023 *Phys. Rev. A* **108** 053314
[25] Verresen R, Lukin M D and Vishwanath A 2021 *Phys. Rev. X* **11** 031005
[26] Ebadi S, Keesling A, Cain M, Wang T T, Levine H, Bluvstein D, Semeghini G, Omran A, Liu J G, Samajdar R, Luo X Z, Nash B, Gao X, Barak B, Farhi E, Sachdev S, Gemelke N, Zhou L, Choi S, Pichler H, Wang S T, Greiner M, Vuletić V and Lukin M D 2022 *Science* **376** 1209
[27] Liu W, Zhang L and Wang T 2023 *Chin. Phys. B* **32** 053203
[28] Fan J, He Y, Jiao Y, Hao L, Zhao J and Jia S 2021 *Chin. Phys. B* **30** 034207
[29] Samani A, El-Fiky E, Morsy-Osman M, Li R, Patel D, Hoang T, Jacques M, Chagnon M, Abadía N and Plant D V 2019 *J. Lightw. Technol.* **37** 2989
[30] Camacho W A, de Carvalho M M, Ramirez J C, de Souza E A T and Saito L A M 2023 *Opt. Laser Technol.* **157** 108622
[31] Deb A B and Kjærgaard N 2018 *Appl. Phys. Lett.* **112** 211106
[32] Anderson D A, Sapiro R E and Raithel G 2021 *IEEE Trans. Antennas Propag.* **69** 2455
[33] Suter D 1997 *The Physics of Laser-Atom Interactions* (Cambridge Studies in Modern Optics)
[34] Scully M O and Zubairy M S 1997 *Quantum Optics* (Cambridge University Press)
[35] Teraji T, Yamamoto T, Watanabe K, Koide Y, Isoya J, Onoda S, Ohshima T, Rogers L J, Jelezko F, Neumann P, Wrachtrup J and Koizumi S 2015 *Phys. Status Solidi (a)* **212** 2365
[36] Holloway C L, Gordon J A, Jefferts S, Schwarzkopf A, Anderson D A, Miller S A, Thaicharoen N and Raithel G 2014 *IEEE Trans. Antennas Propagat.* **62** 6169
[37] IEEE Standard for Ethernet IEEE Std 802.3-2018 (Revision of IEEE Std 802.3-2015) 1–5600
[38] Ehrlichman Y, Amrani O and Ruschin S 2008 *J. Lightw. Technol.* **26** 3567
[39] Chun Y, Megahed M, Ramachandran A and Anand T 2022 *IEEE J. Solid-State Circuits* **57** 1527
[40] Frans Y, Shin J, Zhou L, Upadhyaya P, Im J, Kireev V, Elzeftawi M, Hedayati H, Pham T, Asuncion S, Borrelli C, Zhang G, Zhang H and Chang K 2017 *IEEE J. Solid-State Circuits* **52** 1101
[41] Wang L, Fu Y, LaCroix M A, Chong E and Chan Carusone A 2019 *IEEE J. Solid-State Circuits* **54** 452
[42] Upadhyaya P, Poon C F, Lim S W, Cho J, Roldan A, Zhang W, Namkoong J, Pham T, Xu B, Lin W, Zhang H, Narang N, Tan K H, Zhang G, Frans Y and Chang K 2019 *IEEE J. Solid-State Circuits* **54** 18